Deposition of thermally stable tungsten nitride thin films by reactive magnetron sputtering

A. H. Abdelhameed[1], W. Jacob[*]

Max-Planck-Institut für Plasmaphysik, Boltzmannstr. 2, 85748 Garching, Germany

Abstract

Thermally stable tungsten nitride (W_2N) thin films with thickness $\sim 0.9\ \mu m$ were successfully deposited on Si and graphite substrates by reactive magnetron sputtering. The produced layers show no phase change or nitrogen release up to 1300 K. These novel layers survived annealing at 1200 K for 50 hrs without any measurable nitrogen loss or a phase transition from W_2N to $bcc\ W$. X-ray diffraction, thermal desorption spectroscopy and Rutherford back scattering were utilized to characterize these layers and investigate the nitrogen release mechanism. The micro-structure of the layers was dominated by a grainy structure with porosity less than 16% and a strong texture in (200) orientation in contrast to the common (111) orientation. For annealing temperatures higher than 1200 K nitrogen release was observed, but this was attributed to a chemical reaction of W_2N with the substrate material(s).

Keywords: Tungsten Nitride, Thermal Stability, Magnetron Sputtering, Decomposition, Nitrogen Release

Published in:	Surface & Coatings Technology 375, 701-707 (2019).
doi:	10.1016/j.surfcoat.2019.07.046
Submitted:	18.04.2019
Accepted:	22.07.2019
Available online:	31.07.2019

[*]Corresponding author. Tel.: +49 89 3299 2618; Fax: +49 89 3299 1504. E-mail address: Wolfgang.Jacob@ipp.mpg.de.

[1]Current address: Max-Planck-Institut für Physik, Föhringer Ring 6, 80805, Munich, Germany. E-mail address: aab@mpp.mpg.de.

1. Introduction

Tungsten nitride (WN_x) has attracted quite some interest in the past years due to its unique set of properties, such as excellent hardness, chemical stability, good thermal stability and high electrical and thermal conductivity [1, 2]. That made it a candidate for many potential applications such as Cu diffusion barrier into Si in semiconductor applications [3], wear resistance protective coatings on mechanical components [4], catalyst for nitrogen monoxide dissociation and reduction with hydrogen [5], photoelectrochemical hydrogen production [6] or deuterium diffusion barrier for plasma-facing components in nuclear fusion devices [7]. WN_x thin films have frequently been prepared by reactive magnetron sputtering [4, 7, 8, 9, 10, 11, 12]. The formation of WN_x is thermodynamically unfavorable, especially at atmospheric pressure. Consequently, most of the produced WN_x was in the form of thin films via nonequilibrium processes. The produced layers possessed poor crystallinity, high residual stress and high porosity. Moreover, the reproducibility of such layers was very limited as many parameters can alter the overall properties.

Previous work focused extensively on studying the effects of deposition conditions on mechanical and electrical properties, micro-structure and chemical state configuration of the films. To date, very little is known about the thermal stability and the decomposition behavior of WN_x. Most applications of WN_x often require not only good properties at room temperature, but also stability and functionality at elevated temperatures. Although thermodynamical predictions reported a thermal stability of W_2N up to 2100 K [13], experimental investigations resulted in much lower N_2 release temperatures [10, 11, 12]. Shen et al. [12] reported N_2 release for their films starting at about 1090 K and being fully released at 1170 K. $W{:}N$ films deposited by Gao et al. [11] showed an onset of N_2 desorption at 850 to 900 K and a release peak at 960 to 970 K. Finally, Zhang et al. [10] reported an onset of N_2 release of their magnetron-sputter-deposited W_2N layers at about 600 K continuously increasing and reaching a maximum release rate at about 1200 K. For higher temperatures the release rate dropped strongly to very low values. Obviously the layer decomposed at 1200 K. Furthermore, a dramatic degradation of the layers properties happened at temperatures of about 900 K [4]. So in summary, reported experimental values for the thermal stability of $W{:}N$ layer range from about 900 to 1200 K. On the other hand, high uncertainties in quantifying the nitrogen amount in the deposited films made the study of the correlation of the films composition (stoichiometry), structural details, micro-structure evolution and decomposition behavior ambiguous. That is because of the low cross section of nitrogen in all spectroscopic methods, namely, X-ray photoelectron spectroscopy (XPS) and parallel electron energy-loss spectroscopy (PEELS) .

In this work we show that fabrication of thermally stable thin films by reactive magnetron sputtering is possible by optimizing the deposition parameters. The W_2N layers produced in this work are long term stable for annealing at 1200 K for more than 50 hours. It will further be shown that the observed decomposition at higher temperatures is due to a reaction of the layer with the chosen substrate and not a property of the W_2N layer itself.

2. Experimental

WN_x layers were deposited on single crystal 10×10 mm^2 $Si(100)$ and $12 \times 15 \times 1.5$ mm^3 pyrolytic graphite substrates by reactive magnetron sputtering. Graphite substrates were cut in parallel to the graphite planes and were polished mechanically to achieve surface roughness ~ 0.1 μm. The substrates were then cut and labeled using a laser cutting machine. In case of Si, initial cleaning of the substrates was done using a neutral soap solution followed by washing in a flow of deionized water for 2 min. Soft wiping with dirt-free tissue was applied to fully clean and dry the surface. Finally all the substrates were rinsed vertically in high purity isopropanol in an ultrasonic bath for 10 min and were let to dry out, also vertically.

Depositions were carried out in a commercial Denton Vacuum Discovery-18 device. Prior to deposition, the system was pumped down to a pressure of 4.5×10^{-5} Pa then a cold trap was filled with liquid nitrogen to minimize the water vapor pressure background. The substrate heater was turned on with a heating rate of 20 K/min. The samples were sputter-cleaned for 5 min by Ar plasma of pressure of 1.2 Pa created by applying 100 W RF power to the substrate holder which resulted in a DC self-bias voltage of -500 V.

DC current was applied to a tungsten target with purity of 99.98%. The sputtering process was carried out in a mixture of $Ar - N_2$ atmosphere. Prior to starting the deposition process the sputtering target was also sputter-cleaned for 5 min, with the same gas mixture as used for the deposition. We observed that the W_2N phase could be produced using a wide range of the deposition parameters, however the layers had different properties. Therefore, a series of optimization of the deposition parameters was carried out (not discussed here) to produce the layers explained in this article. The best deposition parameters were found to be: 400 W from power-regulated DC power supply resulted in a target current of 819 ± 5 mA and a sputtering voltage of 420 ± 3 V; the flow rates of Ar and N_2 were set by independent mass flow controllers to be 60 and 15 $sccm$, respectively ($sccm$ stands for cubic centimeter per minute at STP), yielding a total pressure of 2.0 Pa. In the course of the deposition the pressure gradually increased to 2.4 Pa. The distance between the cathode and the substrate holder was fixed at 10 cm (center to center) and the target had an inclination of 25 $^\circ$ since it is a multiple-cathode sputtering system. The deposition time to produce a thickness of 900 ± 20 nm was 40 min.

Independent experiments have shown for layers deposited at low sample temperatures (no substrate heating) nitrogen release sets in at relatively low temperatures ($\sim 750\ K$) [10] . We believe that this release is due to decomposition of some amorphous structures. Therefore, a sufficiently high substrate temperature was chosen for film deposition, aiming to reduce, or prevent, the formation of such amorphous structures with low decomposition temperatures. In the experiments reported here, the substrate temperature was set to be $\sim 800\ K$. The temperature was measured in a separate identical deposition run using a thermocouple pressed against a Si sample while the substrate holder was not rotating, since it was not possible to monitor the sample surface during the rotation of the substrate holder. Layers deposited under the here described conditions with a deposition temperature of $\sim 800\ K$ will be called 'stable layers' in the remainder of this manuscript.

The crystallographic structure and preferred orientation were evaluated by X-ray diffraction (XRD) using a BraggBrentano diffractometer (Philips) in θ-2θ configuration. The X-ray source used the $Cu\ K_\alpha$ line at 0.15418 nm. In front of the source a Ni filter to remove $Cu\ K_\beta$ and a 1.0 mm collimator were used. The diffractometer θ-2θ range was calibrated prior to the measurements with accuracy of 0.0001 °. The samples were scanned in the range of $20-150°$ with a step of 0.01° and counting time of 10 s to enhance the signal-to-noise ratio. Texture measurements were done within χ range of $0-70°$ with step of 5° and ϕ range of $0-360°$ with a step of 10°.

The surface morphology and the micro-structure were evaluated using a scanning electron microscope (SEM, Helios NanoLab 600 from FEI) combined with a focused ion beam (FIB) for cross-section imaging. The residual stress in the deposited films was evaluated by measuring the change of the substrate curvature due to film deposition using a Brukers Dektak stylus profilometer. Annealing up to 1300 K was performed in a full-molybdenum vacuum oven at a pressure of $2.7\times10^{-5}\ Pa$ with a heating and cooling rate of 1 K/min.

Thermal desorption spectroscopy measurements were carried out in a temperature programmed desorption device (explained elsewhere [14]). The sample is placed in a quartz tube inside an external, tubular oven. The oven heating ramp was 15 K/min. Sample temperature calibration was performed separately with a thermocouple attached to the surface of an identical Si sample. The measured sample temperature showed a slight non-linearity up to $\sim 800\ K$. Above $\sim 800\ K$ the sample temperature was linear and about $\sim 20\ K$ lower than the set oven temperature. The base pressure in the TDS system was better than $2\times10^{-8}\ Pa$. Prior to the measurements an identical ramp was performed without sample to desorb molecules which were adsorbed to the quartz tube walls during samples insertion. In addition, the background signal was then measured as a function of temperature and later subtracted from the measured data. The quadrupole mass spectrometer (QMS) was calibrated using two independent methods for D_2 and N_2 gases, namely, by a LACO leak-bottle [15] (D_2 only) and a self-made MINICAN-orifice system described in [16].

Rutherford backscattering spectroscopy (RBS) was carried out using the 3.0 MeV tandem accelerator at IPP Garching, Germany. $3.0-5\ MeV$ ^4He ion beam was used normal to the surface while the backscattering detector was at 165°. Quantifying the nitrogen content in the layers using RBS is of particular importance for the results presented here. However, quantifying light elements in a heavy matrix is not always straight forward. Because the cross section for detection of N is much smaller than that for W, and because the N-related RBS signal for our layer system appears on top of the Si-RBS signal from the Si substrate, the N content cannot be determined directly from the N-RBS signal. But it is possible to determine the N content in the W:N layer from the decrease of the W-RBS signal compared with the W signal of a pure W layer or bulk W if we can assume that N is the only element in the W:N layer that leads to the decrease of the W signal.

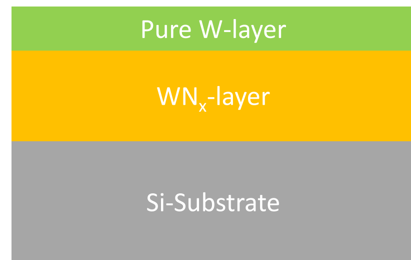

Figure 1: Schematics of the layer-system used to obtain accurate RBS measurements by depositing a thin pure-tungsten layer on top of WN_x.

This method depends on an accurate measure of the absolute W signal height which varies on a day to day basis by about 5 to 10 % due to uncertainties in the ion beam current measurement. Therefore, the such-determined N concentration in the layer has a relatively high uncertainty (of the order of 20-25 % of the determined value). Separate analyses by XPS had shown that the oxygen content in the W:N and pure W layers which are deposited using our setup is negligible. Consequently, we can safely assume that the layers contained only nitrogen. The uncertainty of the N concentration can be significantly reduced, if the W-RBS signal of a pure W layer can be measured simultaneously with the W:N layer. Therefore, we deposited a pure tungsten layer (about 300 nm) on top of the W:N layer as schematically shown in Fig. 1. This pure tungsten layer was deposited in a separate deposition run prior to RBS analysis. The additional pure tungsten layer guarantees that the pure W signal is measured for the identical conditions as the W:N signal, thus decreasing the uncertainty for the determination of the N concentration to about 2 % (of the determined value). For quantitative

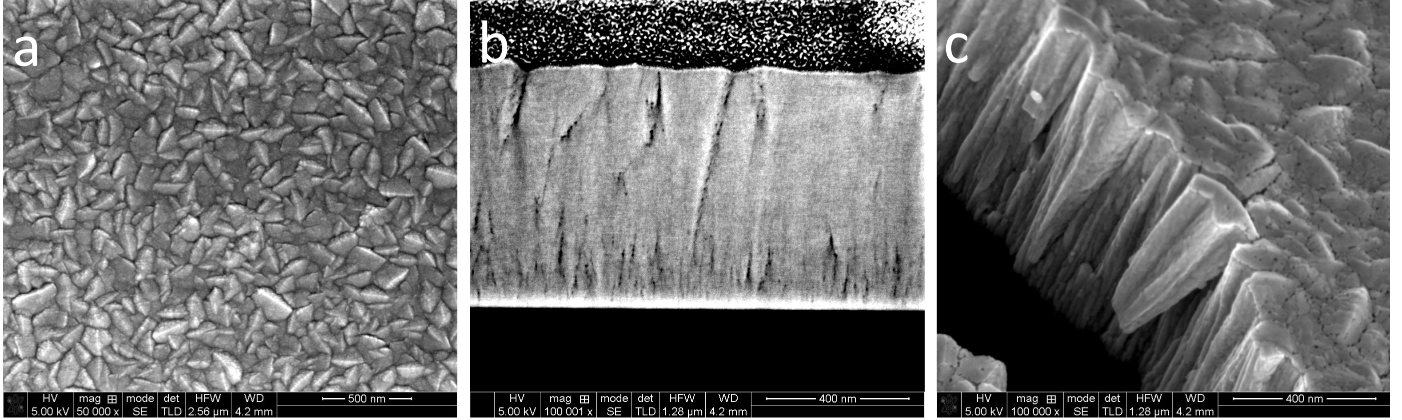

Figure 2: SEM images of stable layers: (a) the surface morphology shows the grainy structure, (b) cross-section made by FIB (vertical scale is 79% of the horizontal scale due to surface tilting), and (c) cross-section image of a crack that occurred after heat treatment shows the columnary structure more clearly.

analysis RBS spectra were evaluated using the SIMNRA code [17].

3. Results

3.1. Film composition and micro-structure

Fig. 2 shows SEM images of the surface morphology of the deposited layers. The structure is dominated by densely packed fibrous grains with structure size $>$ 100 nm. The FIB cross-section image (Fig. 2b) shows the films thickness and a residual minor porosity mainly at the grain boundaries. A further cross-section image of a crack which has developed after heat treatment (Fig. 2c) shows the columnar structure more clearly. Comparison of different surface and cross section images before and after heat treatment did not show a visible change of the columnar microstructure.

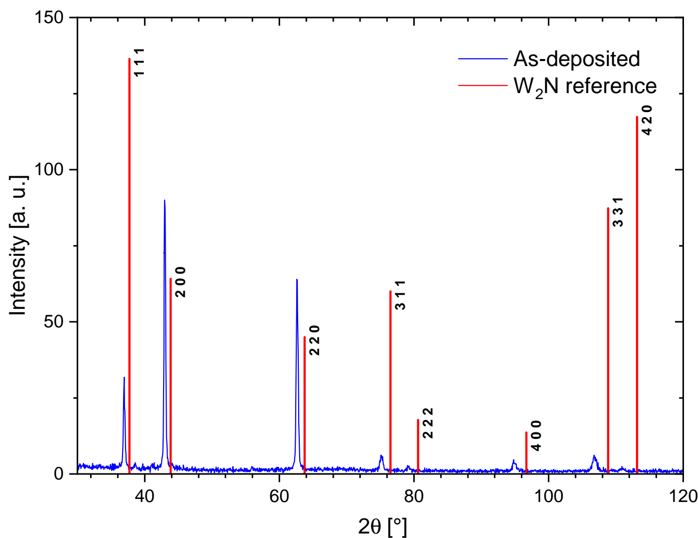

Figure 3: XRD $\theta - 2\theta$ scan of stable W_2N indexed with the reference values (red lines) showing the peak positions and the relative intensities ICDD PDF-2 card 25-1257 [18].

Fig. 3 shows the XRD pattern of the W_2N layers compared with the reference peak-positions and relative intensities from ICDD PDF-2 card 25-1257 [18]. The spectrum shows clearly higher intensities for the (200) and (220) orientation and a strong relative suppression of the (111) orientation compared with the reference spectrum. This means, the layers have a preferential (200) and (220) texture compared with the previously reported preferential (111) texture [9, 10]. In addition, the peaks show a shift towards lower angles (larger lattice plane distance) which indicates a possible tensile residual stress.

Some further information on the films texture is revealed by the pole figures presented in Fig. 4. Shown are pole figures for the three strongest peaks of the diffractogram presented in Fig. 3, namely the (111), (200) and (220) peak. The intensity color scale for the three subfigures is the same. The (200) and (220) peaks shown a fibre texture perpendicular to the sample surface. The mosaic spread of these two diffraction peaks is about 10°. A weak ring at about 45° in the (200) pole figure is a diffraction spot that belongs to the planes with (220) orientation of the (200) grains. A corresponding structure in the (220) pole figure is not well visible. The (111) pole figure shows maximum intensity for a ring at about 27°. This is a diffraction spot that belongs to the grains with (111) orientation tilted by about 27° to the surface normal. The corresponding (111)-plane of the preferential (220)-orientation on the surface texture should appear at 35°. The asymmetry in the intensity distribution for the (111) pole figure is probably due to a non-perfect mounting of the sample on the XRD sample holder.

Furthermore, we calculated the value of the residual stress in the film by measuring the change of the substrate curvature. The such-determined measured stress is found to be tensile and amounts to $\sim 0.35\ GPa$. We believe that the residual stress in this film was mainly due to the thermal stress since the film was deposited at elevated temperatures and the measurements were done at room-temperature. The measured value of the residual

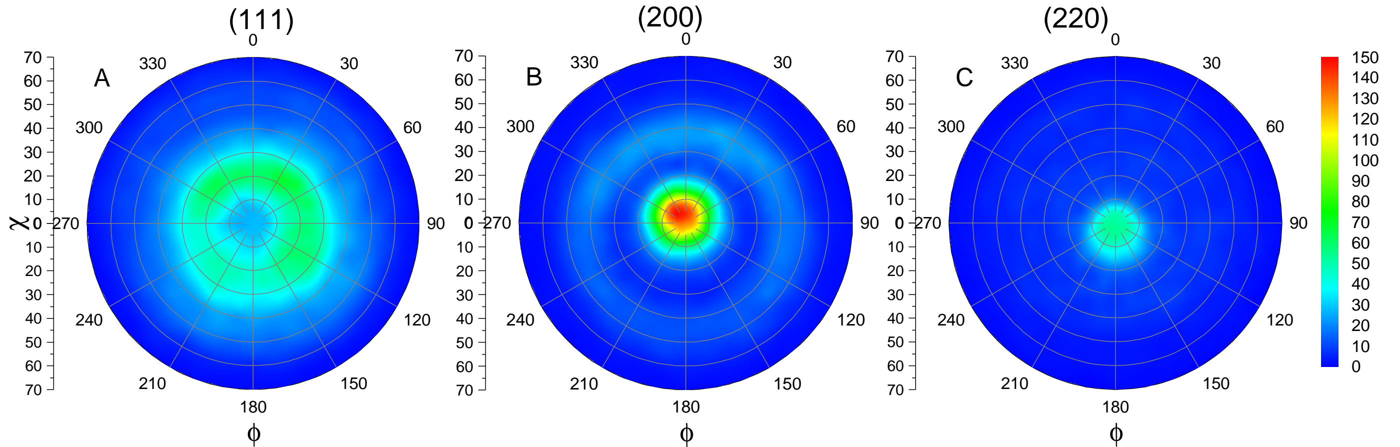

Figure 4: Pole figures showing the crystallographic texture of the layers. The individual figures present the intensities (color maps) of the first three peaks, (111), (200) and (220), as a function of the tilting angle χ and the rotation angle ϕ.

stress was low and in opposite direction compared with the strain needed to shift the positions of the XRD peaks. The stress required to explain the observed peak shift that results in a change in the lattice parameter of 0.016 $\mathring{A}$ is $\sim 9.0\ GPa$ calculated as sum of the principal stresses using [19].

As described in Sec. 2, the N content in the layers was determined by the decrease of the W signal of the W:N layer in comparison with the W signal of a pure W layer. Fig. 5 shows the measured RBS spectrum of an stable W_2N layer and the corresponding simulation result from the SIMNRA fit [17]. The areal densities determined for this W:N layer are 3.81×10^{18} W $atoms/\mathrm{m}^2$ and 2.51×10^{18} N atoms$/m^2$. This results in an N concentration of $40 \pm 2\%$. The anticipated N concentration for stoichiometric W_2N is 33%. Therefore, the experimentally determined N content is about 7 percent points too high which is significantly higher than the experimental uncertainty. We believe that this additional N amount is bonded in amorphous W:N phases with higher N concentration. With other words, that also means that about 17% of the total incorporated N amount in this W:N layer is retained in a non crystalline phase.

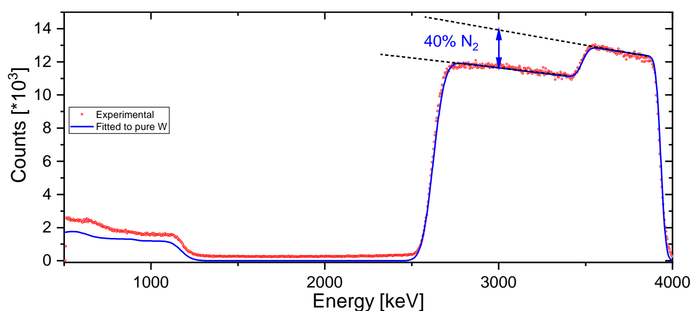

Figure 5: RBS spectrum of the W_2N (red circles) coated with pure-tungsten layer. The blue line represents the SIMNRA simulation result [17].

We estimated the the porosity of the layers from the areal density determined by RBS and the thicknesses determined by SEM on a FIB cross section. The areal densities are given above and the SEM-determined layer thickness for this layer is $900 \pm 20\ nm$. This results in an experimentally determined density of 14.8 g/cm^3. The theoretical value for the W_2N density calculated from the lattice parameters [18] is 17.8 g/cm^3 . The comparison of these two density values results in an average porosity of $\sim 16\%$.

3.2. Thermal stability and nitrogen-release characteristics

Fig. 6 shows a comparison of N_2 desorption rates from two W_2N layers produced in the frame of this work. As mentioned before, the W_2N layer produced applying the deposition conditions described in Sec. 2, in particular the high sample temperature of 800 K during deposition will be called 'stable layer'. The rational for that is the result presented in Fig. 6. The other layer will in the following be named 'common W:N layer'. The deposition conditions for this common W:N layer are: N_2/Ar flow ratio = 30:40 ($sccm$), total pressure of 2.0 Pa, DC power of 300 W resulting in a bias voltage of $\sim 500\ V$ and sample temperature of about 300 K. In general, these deposition conditions are rather similar to reported work [10, 11] and to the conditions for deposition of the stable layer. The main difference for the deposition of the stable layer is the depositon temperature of 800 K instead of 300 K. Although both layers are characterized to be W_2N by XRD, they exhibited completely different thermal stability. The common W:N layer starts to decompose at about 750 to 800 K. The main release peak is at about 970 K and the N_2 release signal has not yet decreased to zero when the maximum temperature for the TDS run has been reached (1323 K).

Unfortunately, we were not able to measure a possible remaining amount of N in the layers after TDS because

the samples were either damaged by peeling off or or suffered from Si diffusion into the layer. However, the integral of the released N amount is in good agreement with the total N amount determined from the RBS analysis prior to TDS. We are, therefore, convinced that the vast majority of the N in the common W:N layer was released during the TDS measurement. On the other hand, the stable layer shows almost no N_2 release in this temperature range. Only a very minor signal becomes apparent above about 1000 K. The thermal stability of this stable layer is further investigated in the following.

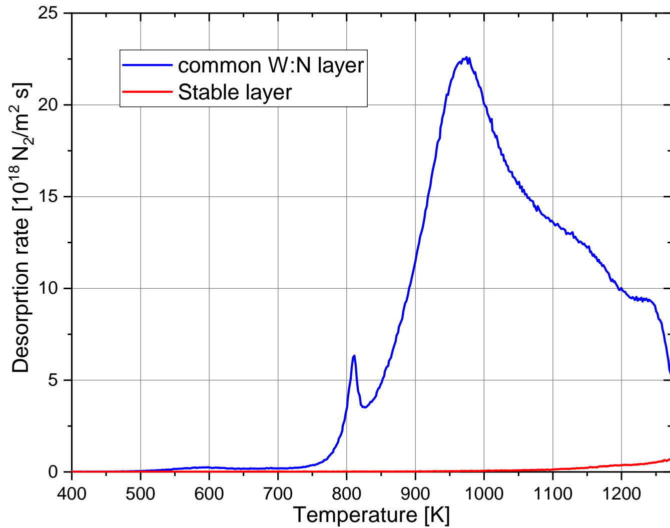

Figure 6: Comparison of the nitrogen release (recorded by the QMS 28 *amu* signal) behavior of the stable layer (red line) vs. a common W:N layer (blue line) as a function of temperature. The released amount is negligible up to 1250 K (only 2.3% of the total amount) whereas almost all the nitrogen from the common W:N layer is released.

Fig. 7 shows the nitrogen release behavior from an approximately 900 nm thick stable W_2N layer deposited on Si as a function of time. Also shown (dashed blue line) is the oven temperature as a function of time. N_2 release sets in at about 1000 K. The release rate increases steeply, resulting in a first peak at about $\sim$ 1250 K and then strongly decreases. This first desorption peak occurs slightly before the maximum temperature in this experiment was reached. After reaching T_{max} (= 1300 K), the sample was held at T_{max} for 3 hours. Surprisingly, during this holding time 2 additional, broad N_2 release peaks occurred. Two points are remarkable: First, the onset of N_2 release as well as the first desorption peak are well above previously reported [10, 11] W:N decomposition temperatures. And second, integrating the N_2 amount released during the ramp up to T_{max} and comparing it with the total released amount we find that the former corresponds to 2.3% only. That means, the vast majority on N_2 released from the sample is released during the holding phase at 1300 K.

As mentioned before in the discussion of the RBS results, the N amount determined by RBS is about 17% higher than anticipated for a pure W_2N phase. We assume that the small amount of N released before reaching T_{max} in Fig. 7 is N released from this non-stoichiometric fraction of N.

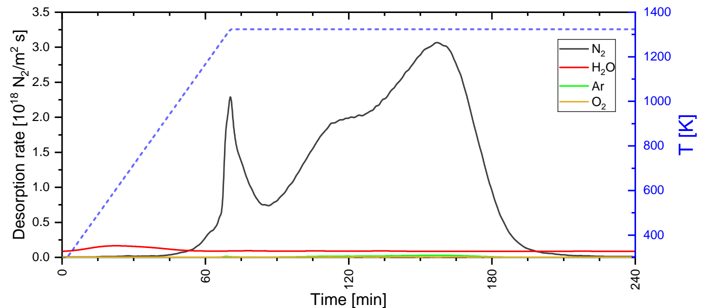

Figure 7: Desorption behavior of H, Ar, H_2O and O_2 from the W_2N sample as a function of time recorded by QMS. One sharp peak visible on the left hand side represents the overstoichiometric nitrogen which is most probably retained in an amorphous phase. It is followed by two overlapping peaks which represent the main nitrogen-release. The dashed blue line shows the oven temperature. The sample temperature is about 20 K lower (see Sect. 2).

In addition to the release of N_2, Fig. 7 shows the desorption behavior of other volatile species. We observed that the sum of all other species was less than 0.5% of the N_2 signal integral. Since all the nitrogen release happened at constant temperature in a relatively slow process of more than two hours, we do not consider that to be a thermal decomposition process.

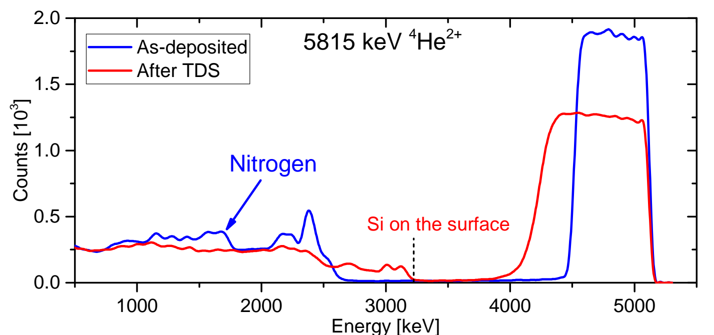

Figure 8: RBS spectrum of the as-deposited W_2N layer in comparison with the RBS spectrum after after TDS to 1300 K and annealing at 1300 K for 3 hours as shown in Fig. 7.

We suggest that the nitrogen release leading to the two broad peaks in Fig. 7 (from about 90 to 180 min) is caused by a diffusion of the substrate material Si into the W_2N layer and a corresponding replacement of N by Si. Fig. 8 shows the RBS spectrum of the layer after the release of all nitrogen during TDS in comparison to the as-deposited spectrum by thermal treatment shown in Fig. 7. The RBS spectrum after annealing changed dramatically: Si is now visible at the surface and simultaneously the W peak became broader while the peak height became lower. Integration over the W peak shows that the total W amount remained constant. The change of the W peak can be ex-

plained by diffusion of Si into the W_2N layer. The weak N peak which is visible in the region around 1500 keV has disappeared after annealing. Together with the observation that the released N amount during the experiment shown in Fig. 7 roughly agrees with the initial N amount measured by RBS prior to annealing we conclude that the layer after annealing contains no significant amount of N. Assuming that the broadening of the W peak is merely due to the diffusion of Si into the W_2N layer - implicitly this also means that N is completely replaced by Si - the W concentration in this layer is $34 \pm 0.5\%$ o. That fits the stoichiometry of WSi_2.

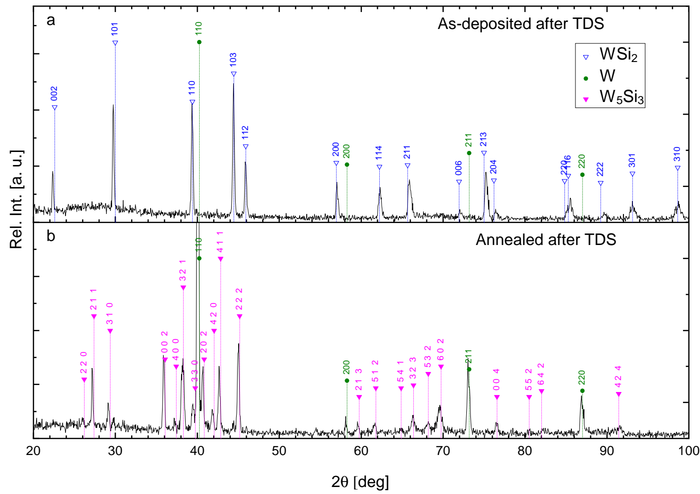

Figure 9: XRD $\theta - 2\theta$ scans of W_2N after TDS and the release of the nitrogen from the as-deposited film (a) and from the annealed film at 1200 K for 50 h (b).

Fig. 9 (top) shows that our XRD scan of the layer after performing TDS (after N is released) fits exactly the WSi_2 from ICDD PDF-2 card 81-165 [18]. The scan is indexed with the peak positions of tungsten to show that no peaks from a pure tungsten phase appeared. Fig. 9 (bottom) shows the XRD pattern, after TDS, of the annealed sample at 1200 K for 50 h. The XRD pattern fits the tungsten siliside phase W_5Si_3 ICDD PDF-2 card 81-165 [18].

The here presented RBS and XRD results consistently show that Si diffuses into the W_2N films and replaces N. The diffusion and replacement is finished after about 3 h annealing at 1300 K. The N from the film is released in form of N_2. This also means that the here observed N release is not due to thermal decomposition of the W_2N film but due to a chemical reaction of the diffused substrate material with the film. We can, therefore, speculate that the thermal stability of the film itself is even higher than 1300 K. Nevertheless, is the here found thermal stability limit of the film-substrate system 300 K higher than the up to now highest reported stability limit.

A comparison was made between the N_2 (mass 28 amu) release signal from TDS measurements of identical layers deposited on Si and graphite substrates. We observed that the nitrogen release from the layer deposited on the graphite substrate was much faster than from the layer deposited on Si. We attribute that to the difference in the diffusion coefficient of Si and C into W [20].

3.3. Annealing effects

In literature, annealing of WN_x showed contradicting results. Some researchers reported crystallization of the amorphous films at temperatures ~ 873 K [9]. However, that was not observed in the course of this study. Since we managed to minimize, to some extend, the amorphous fraction in the films the layers showed higher thermal stability. We performed annealing at 1200 K for 50 h in order to verify the stability of the layers beyond the reported values and to study the heat treatment effects in more detail. Our RBS analysis of the layers after annealing showed a negligible nitrogen loss ($\sim 0.6\%$). The results of our XRD measurements showed neither formation of pure W phase nor a significant change of the crystallinity. However, this annealing had a clear effect on the peak position and we also observed a slight change on the film texture (see Fig. 10). After annealing, the peaks shifted towards the nominal peak position for W_2N and the (200) peak gained strongly in intensity. The former is interpreted as a release of stress and the latter as a change in the film texture. We noticed that a slow heating and cooling ramp (1 K/min in our case) was necessary to relieve the stress without damaging of the film (peeling) as a consequence of a thermal expansion.

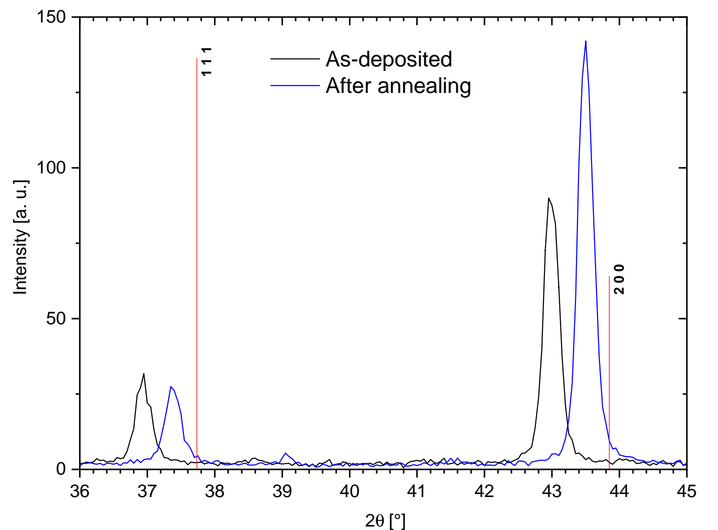

Figure 10: XRD $\theta - 2\theta$ scans of W_2N layers indexed with the reference values. Red lines show the peak positions with relative intensities. Blue line is after annealing at 1200 K for 50 h in comparison with the as deposited layer (black line).

Fig. 11 shows RBS comparison of the layers after heat treatment. We did not notice any change on the layer homogeneity.

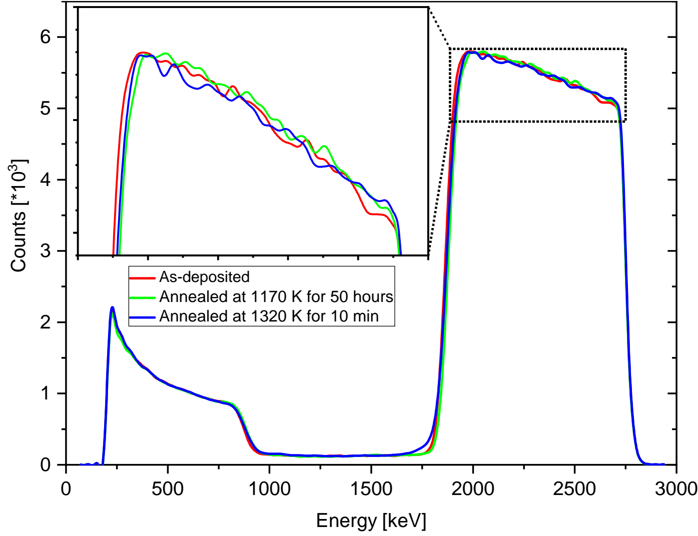

Figure 11: RBS spectra (smoothed raw data) of the W_2N layer as-deposited (red line) and two annealed samples: at 1170 K for 50 h (green line) and at 1320 K for 10 minutes (blue line).

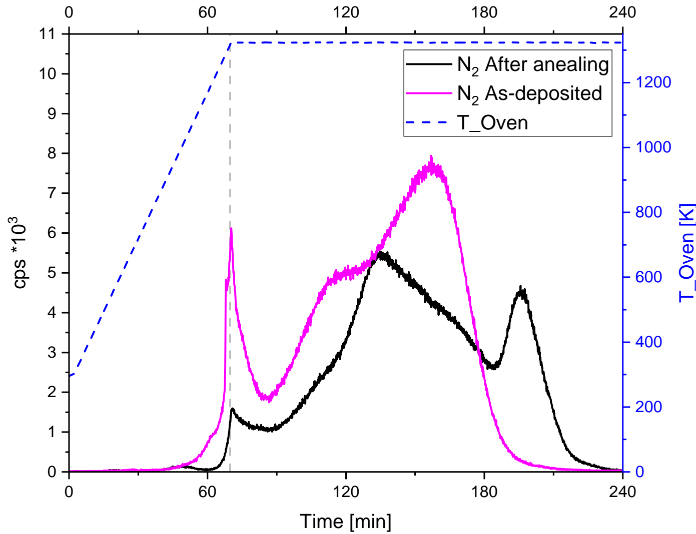

Figure 12: Desorption behaviors of nitrogen as a function of time recorded by QMS for the comparison of two W_2N samples. Black line represents the desorption of the annealed sample in comparison with the desorption of the as-deposited sample.

In order to study the micro-structure changes due to annealing on the nitrogen release behavior, TDS, with the same conditions, was performed on an annealed film. Fig. 12 shows the desorption behavior of nitrogen from the annealed film compared with the desorption from the as-deposited layer. We observed a total delay of the main release of $\sim$ 30 min, in addition to a different release behavior. The interpretation of such observations is not straightforward, however our suggestion is that diffusion of silicon into the film was slower. The observed shift of the XRD peaks (Fig. 10) towards higher angles means that the volume of W_2N lattice was decreased. Together with the enhancement of the crystallinity through the minimization of crystal defects, this might influence the diffusion of silicon into W_2N. Our XRD scan of the annealed film after TDS (Fig. 9 bottom) supports our claim. The XRD peaks show the formation of a tungsten silicide phase W_5Si_3 which has a lower concentration of silicon. In addition, we also observed existence of bcc α-W. That agrees with the phase diagram of Si-W system.

4. Discussion

The thermally stable W_2N layers deposited in this work applying a deposition temperature of 800 K are dense layers with a columnar microstructure (see Fig. **??**). XRD analysis reveals that the layers have a W_2N phase with a preferential (200) and (220) texture (Fig. 3). RBS results are in a reasonable agreement with the predicted atomic concentrations for W_2N stoichiometry which should yield 33% nitrogen. The nitrogen concentration found by RBS is about $40 \pm 2\%$. This additional N concentration of about 7 percent points corresponds to about 17% of the total N amount in the film. The integral over the first release peak at about 1250 K shown in the TDS results in Fig. 7 corresponds to about 15% of the total released nitrogen amount. This value is in a good agreement with the over-stoichiometric nitrogen amount measured by RBS. Taking further into account that the total released N amount is in good agreement with the total N amount measured by RBS, we, therefore, attribute this peak to the release of nitrogen which is either bonded at grain boundaries or in an amorphous phase.

The films exhibit superior thermal stability compared with films deposited at about 300 K (see Fig. 6) and reports from literature [10, 11, 12]. They show no measurable N release for temperature up to 1000 K and only a fraction of about 15% is released up to 1300 K. The influence of long term annealing was investigated at 1200 K for up to 50 h. The N loss measured by RBS (0.6%) was negligible (Fig. 11) and XRD did not show the appearance of another phase (Fig. 9). The only observable effect in the XRD spectrum was a slight peak shift and an increase of the (200) intensity (Fig. 10).

5. Conclusion

Thermally stable W_2N thin films were deposited on Si and C substrates by reactive magnetron sputtering. It is possible to improve the layer properties, especially the thermal stability, by optimizing the deposition conditions. The important deposition parameter identified in our experiments is the sample temperature during deposition. At the here used deposition temperature of 800 K the W_2N films possess superior thermal stability at least up to 1200 K. A release of about 15% of the bonded nitrogen for temperatures after annealing to 1300 K was attributed to a small fraction of N bonded not in the W_2N phase but possibly on grain boundaries or in an amorphous phase.

The observed N release for extended annealing at 1300 K was attributed to a chemical reaction of the here used substrate material (silicon and graphite) into the W_2N layer which leads to a nitrogen release due to a chemical reaction of the substrate material with tungsten. This nourishes the expectation that the decomposition of the W_2N phase occurs at even higher temperatures than 1300 K.

Acknowledgments

The authors would like to thank a number of colleagues at IPP Garching for their continued support for performing the measurements. We thank Joachim Dorner and Michael Fußeder for support regarding the ion beam analysis, Thomas Dürbeck regarding the TDS measurements, Stefan Elgeti regarding the XRD measurements and interpretation, Martin Balden regarding SEM and FIB and Liang Gao regarding the magnetron sputter device.

References

[1] L. Toth, Transition metal carbides and nitrides, Elsevier, 2014.
[2] M. L. Addonizio, A. Castaldo, A. Antonaia, E. Gambale, L. Iemmo, Journal of Vacuum Science & Technology A: Vacuum, Surfaces, and Films 30 (2012) 031506.
[3] J. S. Becker, R. G. Gordon, Applied Physics Letters 82 (2003) 2239–2241.
[4] T. Polcar, N. Parreira, A. Cavaleiro, Wear 265 (2008) 319 – 326. URL: http://www.sciencedirect.com/science/article/pii/S0043164807006916. doi:https://doi.org/10.1016/j.wear.2007.10.011.
[5] C. Shi, X. Yang, A. Zhu, C. Au, Catalysis Today 93-95 (2004) 819 – 826. URL: http://www.sciencedirect.com/science/article/pii/S0920586104003141. doi:https://doi.org/10.1016/j.cattod.2004.06.102, selections from the presentations of the 3rd Asia-Pacific Congress on Catalysis.
[6] V. Chakrapani, J. Thangala, M. K. Sunkara, International Journal of Hydrogen Energy 34 (2009) 9050 – 9059. URL: http://www.sciencedirect.com/science/article/pii/S0360319909014396. doi:https://doi.org/10.1016/j.ijhydene.2009.09.031.
[7] L. Gao, W. Jacob, T. Schwarz-Selinger, A. Manhard, Journal of Nuclear Materials 451 (2014) 352 – 355. URL: http://www.sciencedirect.com/science/article/pii/S002231151400244X. doi:https://doi.org/10.1016/j.jnucmat.2014.04.029.
[8] M. Wen, Q. Meng, W. Yu, W. Zheng, S. Mao, M. Hua, Surface and Coatings Technology 205 (2010) 1953 – 1961. URL: http://www.sciencedirect.com/science/article/pii/S0257897210007310. doi:https://doi.org/10.1016/j.surfcoat.2010.08.082.
[9] Y. Shen, Y. Mai, Surface and Coatings Technology 127 (2000) 238 – 245. URL: http://www.sciencedirect.com/science/article/pii/S0257897200006642. doi:https://doi.org/10.1016/S0257-8972(00)00664-2.
[10] X. Zhang, Y. Wu, B. Mu, L. Qiao, W. Li, J. Li, P. Wang, Journal of Nuclear Materials 485 (2017) 1 – 7. URL: http://www.sciencedirect.com/science/article/pii/S0022311516306523. doi:https://doi.org/10.1016/j.jnucmat.2016.12.009.
[11] L. Gao, W. Jacob, G. Meisl, T. Schwarz-Selinger, T. Höschen, U. von Toussaint, T. Dürbeck, Nucl. Fusion 56 (2016) 016004.
[12] Y. Shen, Y. Mai, W. McBride, Q. Zhang, D. McKenzie, Thin Solid Films 372 (2000) 257 – 264. URL: http://www.sciencedirect.com/science/article/pii/S0040609000010415. doi:https://doi.org/10.1016/S0040-6090(00)01041-5.
[13] B. Predel, N-W (Nitrogen-Tungsten), Springer Berlin Heidelberg, Berlin, Heidelberg, 1997, pp. 1–4. URL: https://doi.org/10.1007/10522884_2144. doi:10.1007/10522884_2144.
[14] E. Salançon, T. Dürbeck, T. Schwarz-Selinger, F. Genoese, W. Jacob, Journal of Nuclear Materials 376 (2008) 160 – 168. URL: http://www.sciencedirect.com/science/article/pii/S0022311508001633. doi:https://doi.org/10.1016/j.jnucmat.2008.02.070.
[15] L. Technologies, Salt Lake City, Utah, USA (2018). URL: www.lacotech.com.
[16] P. Wang, W. Jacob, L. Gao, T. Dürbeck, T. Schwarz-Selinger, Nuclear Instruments and Methods in Physics Research Section B: Beam Interactions with Materials and Atoms 300 (2013) 54–61.
[17] M. Mayer, IPP Report 9/113, Max-Planck-Institut fuer Plasmaphysik, Garching, Germany, April (1997). URL: http://hdl.handle.net/11858/00-001M-0000-0027-6157-F.
[18] International Centre for Diffraction Data PDF-2 2000 (Database), Technical Report, Newtown Square, PA, USA, 2000.
[19] M. E. Fitzpatrick, A. T. Fry, P. Holdway, F. A. Kandil, J. Shackleton, L. Suominen, Determination of Residual Stresses by X-ray Diffraction, Measurement Good Practice Guide 52, National Physical Laboratory, Teddington, Middlesex, United Kingdom, TW11 0LW, 2005. ISSN 1744-3911.
[20] K. Schmid, J. Roth, Journal of Nuclear Materials 302 (2002) 96 – 103. URL: http://www.sciencedirect.com/science/article/pii/S0022311502008073. doi:https://doi.org/10.1016/S0022-3115(02)00807-3.